The role of the temporal pole in temporal lobe epilepsy: A diffusion kurtosis imaging study

Loxlan W Kasa, Terry Peters, Seyed M Mirsattari, Michael T Jurkiewicz, Ali R Khan, Roy A.M Haast

NeuroImage: Clinical 36 (2022) 103201

Contents lists available at ScienceDirect

NeuroImage: Clinical

journal homepage: www.elsevier.com/locate/ynicl

The role of the temporal pole in temporal lobe epilepsy: A diffusion kurtosis imaging study

Loxlan W. Kasa [a,b], Terry Peters [a,b,c,d,1], Seyed M. Mirsattari [c,d,e,f], Michael T. Jurkiewicz [c,d,e], Ali R. Khan [a,b,c,g,1,*], Roy A.M Haast [g,2]

[a] Imaging Research Laboratories, Robarts Research Institute, London, Ontario, Canada
[b] School of Biomedical Engineering, Western University, London, Ontario, Canada
[c] Department of Medical Biophysics, Western University, London, Ontario, Canada
[d] Department of Medical Imaging, Western University, London, Ontario, Canada
[e] Department of Clinical Neurological Sciences, Western University, London, Ontario, Canada
[f] Department of Psychology, Western University, London, Ontario, Canada
[g] Centre for Functional and Metabolic Mapping, Robarts Research Institute, Western University, London, Ontario, Canada

ARTICLE INFO

Keywords:
Temporal lobe epilepsy
Temporal pole
Diffusion kurtosis imaging
Automated fiber-tract quantification
Tract-based cortical analysis

ABSTRACT

This study aimed to evaluate the use of diffusion kurtosis imaging (DKI) to detect microstructural abnormalities within the temporal pole (TP) and its temporopolar cortex in temporal lobe epilepsy (TLE) patients. DKI quantitative maps were obtained from fourteen lesional TLE and ten non-lesional TLE patients, along with twenty-three healthy controls. Data collected included mean (MK); radial (RK) and axial kurtosis (AK); mean diffusivity (MD) and axonal water fraction (AWF). Automated fiber quantification (AFQ) was used to quantify DKI measurements along the inferior longitudinal (ILF) and uncinate fasciculus (Unc). ILF and Unc tract profiles were compared between groups and tested for correlation with disease duration. To characterize temporopolar cortex microstructure, DKI maps were sampled at varying depths from superficial white matter (WM) towards the pial surface. Patients were separated according to the temporal lobe ipsilateral to seizure onset and their AFQ results were used as input for statistical analyses. Significant differences were observed between lesional TLE and controls, towards the most temporopolar segment of ILF and Unc proximal to the TP within the ipsilateral temporal lobe in left TLE patients for MK, RK, AWF and MD. No significant changes were observed with DKI maps in the non-lesional TLE group. DKI measurements correlated with disease duration, mostly towards the temporopolar segments of the WM bundles. Stronger differences in MK, RK and AWF within the temporopolar cortex were observed in the lesional TLE and noticeable differences (except for MD) in non-lesional TLE groups compared to controls. This study demonstrates that DKI has potential to detect subtle microstructural alterations within the temporopolar segments of the ILF and Unc and the connected temporopolar cortex in TLE patients including non-lesional TLE subjects. This could aid our understanding of the extrahippocampal areas, more specifically the temporal pole role in seizure generation in TLE and might inform surgical planning, leading to better seizure outcomes.

1. Introduction

Temporal lobe epilepsy (TLE) is the most common form of medically intractable focal epilepsy in adults (Engel, 2006; Georgiadis et al., 2013). In most of these patients, the seizure onset zone lies within the mesial temporal lobe, which is commonly induced by mesial temporal sclerosis (MTS), including hippocampal sclerosis (Chabardès et al., 2005; Jehi et al., 2015). Studies have shown, in clearly delineated MTS using both MRI (i.e., in MRI positive or 'lesional TLE' patients) and scalp EEG, that nearly 80 % of patients are seizure-free after resective surgery

* Corresponding author at: Department of Medical Biophysics, Canada Research Chair (Tier II) in Computational Neuroimaging, Schulich School of Medicine and Dentistry, Western University, Robarts Research Institute, Rm. 1240A, 1151 Richmond St N, London, ON N6A 5B7, Canada.
E-mail address: alik@robarts.ca (A.R. Khan).
[1] shared senior authorship.
[2] current affiliation: Aix-Marseille University, CNRS, CRMBM, UMR 7339, Marseille, France.

https://doi.org/10.1016/j.nicl.2022.103201
Received 29 April 2022; Received in revised form 13 September 2022; Accepted 14 September 2022
Available online 14 September 2022

(Abel et al., 2018). Nevertheless, full delineation of pathological tissue can be challenging since seizures are not always exclusive to the hippocampus, but may rather originate from extrahippocampal structures (Chabardès et al., 2005). Thus, the epileptogenic zone may extend beyond the atrophic mesial temporal structures and explain long-term recurrence of seizures after selective resections (Berkovic et al., 1995). A growing body of clinical investigation suggests that, among other extrahippocampal structures possibly involved in seizures, the temporal pole (TP, i.e., Brodmann's Area [BA] 38 or anterior temporal lobe) could play an important and potentially underappreciated role in TLE (Abel et al., 2018; Thom et al., 2009). The TP is connected to the three temporal gyri, while the two association fibers that terminate at the TP provide connections to the prefrontal cortex (i.e., uncinate fasciculus (Unc)) and amygdala and hippocampus (i.e., inferior longitudinal fasciculus (ILF)), consequently associating with several functions including memory (Catani and Thiebaut de Schotten, 2008; Wong and Gallate, 2012). Also, diffusion-weighted imaging (DWI) studies have consistently shown TLE to be a network disorder with underlying microstructural alterations in the temporal and extra-temporal white matter (WM) fiber bundles, supporting stereoelectroencephalography-based findings of wide-spread cortical involvement (Bartolomei et al., 2017). Similarly, diffusion anomalies have also been detected in the cortical gray matter (GM) and superficial white matter (SWM, i.e., the WM area directly bordering the GM) (Liu et al., 2016; Lorio et al., 2020; Sone et al., 2018; Winston et al., 2020). Each of these separate studies found microstructural irregularities in the temporal pole, as depicted in the change of diffusion tensor imaging (DTI) parameters and decreased fiber density measured with neurite orientation dispersion and density imaging. Despite these promising findings using DWI, a substantial portion of TLE patients (~30 %) – often referred to as 'non-lesional' (or MRI negative) TLE patients – do not show lesions in their MRI scans, which can complicate the presurgical workup in these cases.

Although DTI is an elegant tool with relatively straightforward imaging requirements, a considerable number of studies (e.g., (Tournier et al., 2011) and references therein) have shown it to be inadequate for quantifying regions with complex fiber configurations (e.g., crossing fibers) (Tournier et al., 2011). As such, a technique called diffusion kurtosis imaging (DKI) was developed to address the DTI shortcomings that prevent it from accurately quantifying complex microstructure (Jensen et al., 2005). DKI enables the measurement of free diffusion (i.e., via its derived DTI metrics) and restricted diffusion within complex microstructure as it provides the common mean diffusivity (MD) and fractional anisotropy (FA) parameters, as well as different kurtosis measures, namely mean kurtosis (MK); radial kurtosis (RK); axial kurtosis (AK); and kurtosis fractional anisotropy (Kfa) (Jensen et al., 2005; Wu and Cheung, 2010). (Bonilha et al., 2015; Glenn et al., 2016) showed that these DKI-derived metrics are sensitive to WM network and GM abnormalities associated with TLE. Furthermore, DKI can also be used to calculate specific microstructural compartments such as the ratio of axonal water content and the total water content per voxel, also known as axonal water fraction (AWF) (Fieremans et al., 2011; McKinnon et al., 2018). Therefore, DKI could provide a complementary and more comprehensive characterization of diffusion in complex tissue environments, and potentially be more sensitive to diffusion anomalies in TLE patients compared to the more commonly employed DTI acquisition. However, the benefit of DKI for detecting subtle alterations in the microstructure of the TP in TLE, including non-lesional TLE, has yet to be established.

The work described in this paper aims to evaluate the sensitivity of DKI to detect abnormalities at specific regions along the two association WM fiber bundles, ILF and Unc connected to the TP and the connected temporopolar cortex in lesional and non-lesional TLE patients. We believe that a better understanding of the microstructural properties of the TP in TLE patients could improve the planning of resective surgeries and their outcomes.

2. Materials and methods

2.1. Subjects

The study was approved by the research and ethics board at Western University and informed consent was obtained from all patients and the healthy control subjects prior to their recruitment in the study, following the Declaration of Helsinki. The patient cohort was selected based on the following inclusion criteria: (a) history of TLE; (b) clinical 1.5 T MRI, and (c) comprehensive EEG studies completed to identify the site of their epileptogenic region. On the other hand, a patient who: (a) had a pacemaker or other electronic or (b) metallic implants; (c) were pregnant or trying to conceive, or (d) had pre-existing medical conditions was excluded. Since the clinical epilepsy protocol MRI is performed at 1.5 T at our institute, T1w and FLAIR images from our subsequent 3 T MRI research protocol were assessed radiologically (M.T.J), blinded to any clinical data of the patients. Of the 24 TLE patients recruited in this study (9 females, mean age ± SD = 32 ± 10 years), 10 were considered non-lesional TLE (i.e., patients not showing any signs of lesions in their MRI structural scans, 4 female, 27 ± 6 years). Twenty-three healthy controls (14 female, 36 ± 15 years) without any history of neurological and psychiatric disease underwent the same neuroimaging protocol. Thirteen patients had undergone temporal lobectomy (i.e., 6 right and 7 left hemisphere) and further investigation with post-surgical pathology confirmed the presence of MTS and gliosis in more than 75 % of this group. A detailed description of the demographic and clinical information for patients included in this study is provided in Table 1. Fig. 1 below outlines the main steps of the workflow in this study, each are discussed in detail in the following subsections.

2.2. MRI acquisition and processing

All subjects were scanned using a 3 T MRI system (Siemens Prisma, Erlangen Germany) with a 32-channel head coil. The scanning protocol included the acquisition of structural images using a magnetization-prepared rapid acquisition with gradient echo (MPRAGE) sequence (repetition time/echo time TR/TE = 5000/2.98 ms, 700 ms TI, FOV = 256x256mm^2, 1 mm isotropic voxel size).

In addition, a multiband echo-planar imaging (*EPI*) sequence with acceleration factor = 3 was used to acquire diffusion-weighted images (DWI). The DWI acquisition includes b = 0, 1300, 2600 s/mm^2, 130 diffusion-encoding directions acquired twice with left–right, right-left phase encoding directions, TR/TE = 2800/66.80 ms, FOV = 224 × 224 mm^2, and 2 mm isotropic voxel size. The acquired diffusion-weighted images were corrected for *EPI* readout and eddy current distortions using *topup* (Andersson et al., 2003) and *eddy* (Andersson and Sotiropoulos, 2016) from FSL (Smith et al., 2004). Correction of Gibbs' ringing artifact was performed by determining optimal sub-voxel shifts within the neighborhood of sharp edges in the image (Kellner et al., 2016), while noise reduction was achieved by separating the signal from the noise in the image via local noise estimation (MRtrix3's *dwidenoise*) (Tournier et al., 2012; Veraart et al., 2016) (Fig. 1A step (i) of the general workflow).

2.3. Calculations of DKI parameters

As part of step (i) in Fig. 1A, the preprocessed DWIs were used as input to the open-source Diffusion Kurtosis Estimator (DKE) software package to calculate the DKI parameters (MK, AK, RK, Kfa) including MD and FA derived from DKI (Tabesh et al., 2011). In addition, we modeled the AWF metric from the kurtosis tensor using the DKE software (Fieremans et al., 2011).

2.4. Automated white matter fiber quantification

The automated fiber-tract quantification (AFQ) software (Yeatman

Table 1
Clinical characteristics of patients with left and right temporal lobe epilepsy.

ID	Age	Sex	Hand	MRI Findings	Intracranial EEG Sz. Location	Scalp EEG Sz. Location	Hipp. path	Neo.path	Duration (years)	Follow up (months), Engel outcome	Sz. Frequency
1	43	M	R	NL	L Temporal-Occipital	N/A	N/A	N/A	<1	*	Daily
2	21	M	R	NL	N/A	L Temporal Lobe	Gliosis	Gliosis	2	60, IA	Weekly
3	22	F	R	NL	L Parietal-Opercular	L Central or non-Localizable	N/A	N/A	1	*	Daily
4	34	M	R	NL	R anterior-inferior insula plus anterior-hippocampus	R Temporal Lobe	Gliosis	Gliosis	4	40, IA	Weekly
5	27	M	R	NL	Indep. L Insula	R Temporal Lobe	N/A	N/A	11	*	Weekly
6	28	F	R	NL	R Temporal Lobe	R Temporal Lobe	Gliosis	Gliosis	2	48, IIA	Weekly
7	21	M	R	NL	L Temporal Lobe	L Temporal Lobe	Gliosis	Gliosis	2	42, IIA	Monthly
8	23	M	L	NL	N/A	R Temporal Lobe	Reactive Changes	Gliosis	4	33, IIA	Weekly
9	29	M	R	NL	L Anterior Mesial Temporal	L Fronto-Temporal Lobes	Gliosis	Gliosis	5	34, IA	Monthly
10	26	F	R	NL	R para-central	None	N/A	N/A	15	*	Weekly
11	26	F	L	Bilateral MTS	Bitemporal	R Fronto-Temporal Lobes	N/A	N/A	24	*	Monthly
12	27	M	R	R DNET	N/A	R Temporal Lobe	FCD/MTS/ Gliosis	FCD/ MTS/ Gliosis	26	57, IIA	Monthly
13	18	M	R	L FCD	L Insular	Independent bitemporal	Scars	Gliosis	6	44, IIA	Monthly
14	48	M	R	R hippocampus atrophy	N/A	R Temporal Lobe	N/A	N/A	1	*	Monthly
15	53	M	R	L MTS	N/A	L Hemisphere (Diffuse)	MTS	Gliosis	11	4, IIA	Weekly
16	52	M	R	L MTS	N/A	L Fronto-Temporal Lobes	N/A	N/A	48	*	Monthly
17	42	M	R	L MTS	N/A	L Temporal Lobe	Gliosis	Gliosis	7	51, IIIA	Weekly
18	31	F	R	L MTS	N/A	L Temporal Lobe	MTS	Gliosis	27	39, IIA	Weekly
19	21	F	R	R amygdala FCD	N/A	R Temporal Lobe	Gliosis	Gliosis	12	23, IA	Monthly
20	51	F	R	R MTS	N/A	R Anterior Mesial Temporal Lobe	N/A	N/A	40	*	Monthly
21	37	M	R	R MTS	N/A	R Temporal Lobe	MTS/ Gliosis	MTS/ Gliosis	35	29, IIA	Weekly
22	36	F	R	R MTS	R Anterior Mesial Temporal Lobe	R Insular	MTS	Gliosis	16	23, IA	Weekly
23	30	F	R	R MTS	N/A	R Temporal Lobe	N/A	N/A	9	*	Weekly
24	26	M	R	R MTS	N/A	R Temporal Lobe	N/A	N/A	5	*	Weekly

MRI Findings – From 3 T MRI, **DNET** – Dysembryoplastic Neuroepithelial Tumor, **FCD** – Focal Cortical Dysplasia, **L** – Left, **R** – Right, **MTS** – Mesial Temporal Sclerosis, **NL** – normal MRI, **Sz** – Seizure, and * – Not a Surgical Candidate, **N/A** – not available.

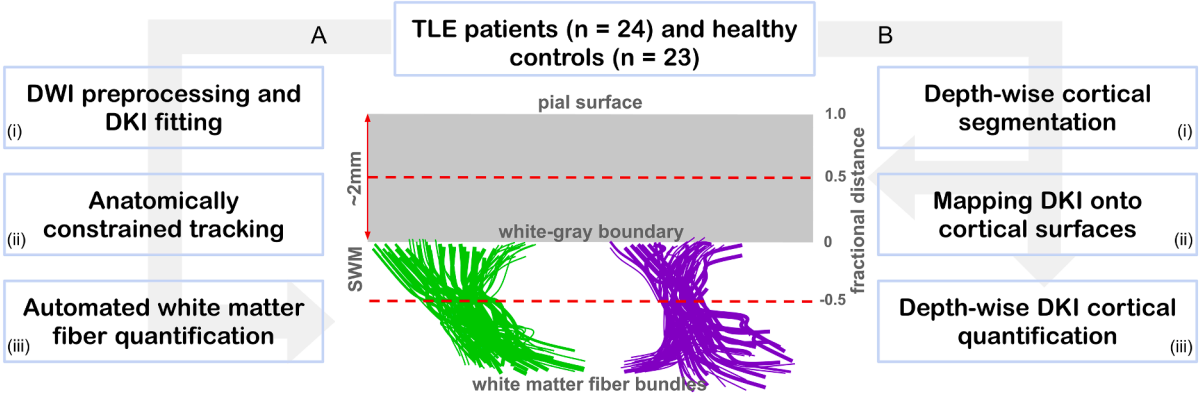

Fig. 1. General data processing workflow. Twenty-four patients and 23 healthy controls were recruited for the study. The tract-based DKI analysis processing stream (A) involved (i) DWI data preprocessing and generating of DKI parametric maps, (ii) white matter fiber bundles (illustrated in green and purple) extraction using anatomically constrained tracking and (iii) white matter fiber bundle profiling. The tract-based cortical analysis (TCA) stream (B) involved (i) extraction of depth-wise surfaces ranging from superficial white matter (SWM, i.e., at −0.5 fractional distance) towards the pial surface (i.e., 1.0 fractional distance), (ii) quantitative mapping of DKI parametric maps to allow (iii) cortical quantification. (For interpretation of the references to color in this figure legend, the reader is referred to the web version of this article.)

et al., 2012) was used to quantify the WM fiber bundles of interest (i.e., ILF and Unc). The basic AFQ four-step procedure was executed: (i) fiber tractography, (ii) fiber tract segmentation using two waypoint regions of interest (ROIs), (iii) fiber tract refinement via a probabilistic fiber tract atlas, and (iv) sampling diffusion measurements at 100 equidistant points along the tract length between two waypoints. To accommodate complex fiber configurations (i.e., fiber crossings) we modified the steps (i) and (ii) of the AFQ workflow, and each of these steps is described in more detail in the following respective subsections (2.4.1–2.4.3).

2.4.1. Fiber tracking and segmentation

We used the anatomically constrained tracking (ACT) algorithm (Smith et al., 2012) implemented in MRtrix3 software (Tournier et al., 2012) (Fig. 1A, step ii). In ACT, the first step is to calculate a response function, which was estimated from the pre-processed DWIs using *dwi2response* (with the "dhollander" algorithm for multi-shell data) (Dhollander and Connelly., 2016). In the second step, the estimated response functions for individual DWIs were used to calculate the fiber orientation function (FOD) using *dwi2fod*. The FODs were separately calculated for the three tissue types (i.e., WM, GM, and cerebrospinal fluid (CSF)) using the multi-shell multi-tissue constrained spherical deconvolution (CSD) method (*msmt_csd*) (Jeurissen et al., 2014). To allow for group comparison, the subjects' WM FODs were input to the *population_template* function to generate an unbiased group average FOD template, to which the respective subject's FODs were warped. To deploy the ACT algorithm, additional anatomical information is required to guide the termination and acceptance/rejection criteria during fiber tracking in MRtrix3 (Smith et al., 2012). Individual subject's T1 images were segmented into five tissue types ('5TT'), namely: WM, subcortical GM, GM, and CSF, and the optional tissue type (i.e., pathological tissue, which was excluded here), using MRtrix3's *5ttgen* command. This function uses FSL's FIRST and FAST segmentation algorithms to separate the four mandatory tissue types. To minimize tracking into the deep GM, we generated a WM-GM interface mask by inputting the 5TT segmented anatomical image into the *5ttgmwmi* command. The resulting WM-GM interface mask was used as seed point for tracking. To further guide fiber tracking, extra parameters were supplied to the MRtrix *tckgen* function responsible for tractography, following the six criteria described by Smith et al. (2012). These parameters influence the streamlines in two ways: when to terminate them and when they are either accepted or rejected based on their biological plausibility. Since tracking was seeded in the WM-GM interface, inclusion and exclusion waypoint ROIs for the bundles ILF and Unc in both hemispheres were inputted as part of step 3 of the devised six steps, as described by Smith et al. (2012). This removed any anatomically implausible tracts by only allowing tracks that pass through the waypoint (Horbruegger et al., 2019; Smith et al., 2012). These waypoint ROIs were defined in MNI152 space and coregistered to the FOD template through a non-linear transformation hereby using the subject's native FOD space as an intermediate step followed by warping to the FOD template using the warps calculated during *population template* stage. Thus, no manual drawing of the ROIs for each subject was required each time when running ACT. The registration was manually checked before inputting the ROIs into the ACT algorithm. Finally, for tracking, we used the *tckgen* iFOD2 algorithm, which is capable of reconstructing fibers with complex configurations (Tournier et al., 2010). We used the following additional *tckgen* settings and inputs: step size 0.8 mm, min. length = 8 mm, max. length = 250 mm, max. number of streamlines = 10,000, unidirectional, include = inclusion ROI, exclude = exclusion ROI and seeding and cropped at GM-WM interface, with latter crop streamline more precisely as they cross WM-GM interface.

2.4.2. Fiber tracts refinement and cleaning

The generated tracts using ACT were refined by comparing each candidate fiber bundle (i.e., ILF and Unc) to their respective probability maps provided within the AFQ tool (Yeatman et al., 2012) (within step (iii) of Fig. 1A). As part of the AFQ processing, the probability maps are transformed into FOD template space. The ILF and Unc are assigned scores based on the probability values of the voxels through which they pass. Any trajectories with low probability scores are discarded. Here, the AFQ fiber probabilities were computed using the atlas procedure of (Hua et al., 2008). Basically, each fiber point probability score is determined by looping over the fiber probability maps, a mean is calculated by collapsing the scores across all points in a fiber. To categorize the fibers, the mean fiber probability score gets sorted, fibers with the highest score after sorting gets selected discarding any fibers with lower scores or does not match the probability maps (Yeatman et al., 2012). Finally, the selected ILF and Unc bundles should pass through the two predefined AFQ waypoint ROIs and also conform to the shape of the respective tract's probability map. In addition, the fiber tracts are cleaned further by determining the core of the fiber tracts to identify and remove any stray fibers. A fiber is represented as a 3D Gaussian distribution, and any outliers in the distribution are discarded (see Fig. 2 for an example of the processed tracts).

2.4.3. Sampling diffusion measurements along WM tract lengths

The diffusion measurements were sampled along subject-specific ILF and Unc fiber cores at 100 equidistant points (Fig. 1A, step iii), allowing for inferences to be made at approximately identical locations across subjects, independent of brain size. This provided the respective tract profiles for each DKI map (MK, AK, RK, Kfa, MD, FA, and AWF) from the individual subjects, and from which the diffusion status in the WM can be inferred. Furthermore, to verify that diffusion profiling was restricted to WM and not contaminated with the signal originating from GM, we calculated the signed distance to the WM-GM boundary for each WM voxel, with negative values indicating proper sampling (see Fig. 5A). For group-wise statistical analyses, each patient group was separated according to the side of lesion for lesional TLE subjects, and the side of seizure focus, identified with comprehensive EEG investigations for non-lesional TLE subjects (i.e., separated according to side ipsilateral to the epileptogenic temporal lobe), and their AFQ results were used as input to the Permutation Analysis of Linear Models (PALM) toolbox (see also section 2.7 on statistical analyses).

In addition, the changes of diffusion properties along the fiber bundles were summarized using the first four statistical moments: mean (i.e., mean of quantitative values, mean(y) and center of gravity in the x-direction, mean(x)), standard deviation (SD), skewness and kurtosis (Amunts et al., 1999). These summary metrics provide further information on any systematic change in the properties of the underlying microstructure along the respective white matter tracts (DeKraker et al., 2020).

2.5. Correlation between combined DKI metrics and disease duration

Since DKI quantifies both the Gaussian component of diffusion (i.e., DTI metrics) and the non– Gaussian component (i.e., DKI metrics), we performed a combined DKI quantitative analysis (e.g., MD + MK). In addition, we incorporated the patient's disease duration (i.e., time between age of onset and age at scan) to investigate its correlation with different combinations of the DKI metrics. The DKI metrics were extracted from two segments of the bundles: the temporopolar segment (i.e., sampling points 80–99) and the remaining non-temporopolar part (i,e., sampling points 0–79). The points 0–79 and 80–99 were selected to obtain bundle segments more distal and proximal to the temporal pole, respectively. This cut-off value (i.e., 80) was determined based on distance to GM, z-score transitions and empirical testing across different cut-off values (70–90). The latter did not reveal strong dependency.

2.6. Tract-based cortical analysis

To quantify diffusion profiles along the ILF and Unc to pial GM axis –

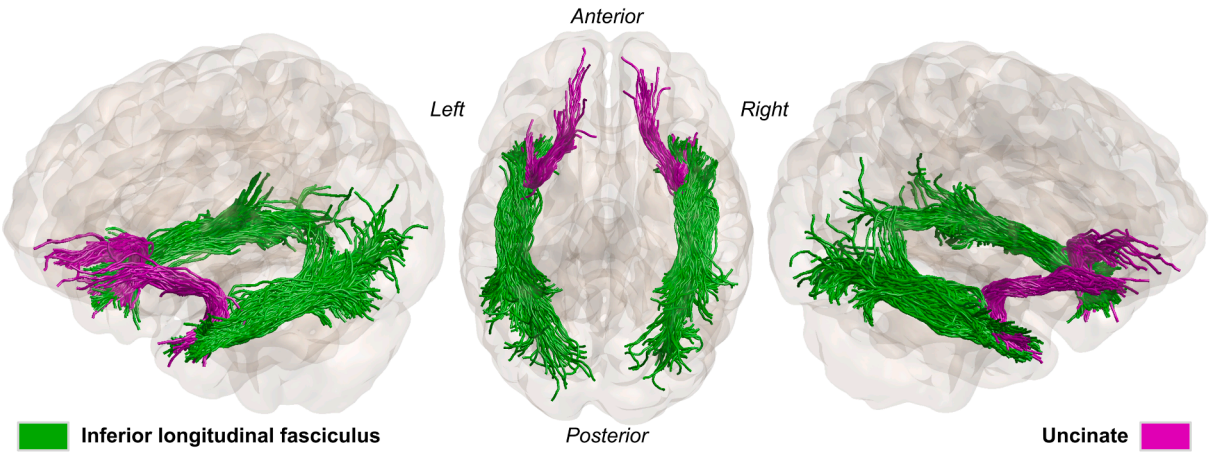

Fig. 2. The two white matter fiber bundles of interest, inferior longitudinal (green) and uncinate fasciculus (purple) for a representative healthy subject. Generated using anatomically constrained tractography and processed with AFQ. (For interpretation of the references to color in this figure legend, the reader is referred to the web version of this article.)

referred to forthwith as tract-based cortical analysis (TCA) (see Fig. 1 stream B) – we mapped all the individual subject's DKI maps onto a series of cortical surfaces. First, a surface-based representation of the cortex was constructed using FreeSurfer's *recon-all* pipeline and the MPRAGE T_1w volume. The resulting WM surface was then used to obtain the additional cortical surfaces using FreeSurfer's *mris_expand* function. These were positioned at different depth fractions based on the estimated local (i.e, vertex-wise) cortical thickness, starting with a 'superficial' WM surface (-50 % of cortical thickness with respect to WM-GM boundary) up to the pial GM (+90 % of cortical thickness) with steps of 10 %, resulting in a total of 15 surfaces while maintaining smoothness and preventing self-intersection (Fig. 1B step (i)). FreeSurfer's *mri_vol2surf* function was then used to project the DKI maps in anatomical space onto each of the generated surfaces (Fig. 1B step (ii)). The cortical reconstructions and coregistration of DKI maps were visually checked by overlaying the WM and pial surfaces onto the resampled B0 data to assure accurate surface mapping. No manual corrections of cortical surfaces and/or registrations were required. Due to limiting voxel size and partial volume effects, only values up to 50 % (i.e., 0.5 or mid-GM, see Fig. 1) are considered for interpretation. Finally, vertex-wise DKI data were averaged within the rostral middle frontal (RMF) and temporal pole cortical regions (defined by FreeSurfer's cortical parcellation) at each depth fraction per subject to allow comparison of profiles across groups (Fig. 1B step (iii)). The RMF was included to serve as a baseline, as we expected little to no effects relating to TLE in this area. Similar to the WM analysis, for group-wise statistical analyses, each patient group (i.e., lesional TLE and non-lesional TLE) was separated according to the side of the epileptogenic temporal lobe (i.e., ipsilateral to the seizure focus). Hereafter, left lesional TLE and non-lesional TLE refer to left TLE patients with or without structural changes in the left temporal lobe, respectively. Similarly, right lesional TLE and non-lesional TLE refer to right TLE patients with or without structural changes in the right temporal lobe, respectively. Note, patients showing potential of bilateral lesions were lateralized according to their EEG findings.

2.7. Statistical analysis

The PALM toolbox was used to statistically assess group-wise differences in terms of WM profiles for each of the individual DKI-derived and WM distance maps using recommended parameters (Winkler et al., 2014). A total of N = 5000 permutations was used together with a cluster-wise *t*-statistic threshold of 3.1, while correcting for multiple comparisons (i.e., locations along the bundle) using the familywise error (FWE, q-FWE = 0.05), as well as age and sex effects. Output *p*-values were saved as -log10(*p*) for visualization. The *statsmodels* (v0.12.2) Python package was used for the comparison of WM profile shapes across groups using one-way analysis of variance (ANOVA), and between bundles (within-subjects) using repeated-measures ANOVA. As for the WM bundles, age and sex were accounted for by including them in the statistical models as additional regressors. Similarly, ANOVA testing was used for contrasting WM bundle summary scores between lesional TLE and non-lesional TLE as well as diffusion parameter maps, while linear regression was used for testing the correlation with disease duration. Since the main objective of the current manuscript was to highlight (i) the added value of DKI and (ii) the involvement of the temporal pole in TLE, robust assessment of the exact clinical impact across a wide array of TLE 'types' (i.e., lesions vs non-lesional, different pathologies) would require a more multi-disciplinary approach and a larger sample size and therefore is beyond the scope of this article.

3. Results

3.1. White matter quantitative profiling

DKI quantitative profiles and corresponding z-scores (shown as heat maps) for the lesional TLE subjects (i.e., left and right TLE patients with structural changes), compared to the healthy controls, are shown in Fig. 3. Ipsilateral to the seizure focus, significant differences were observed between lesional TLE and controls ($p < 0.005$) towards the most temporopolar segment (i.e., position 99) of the left ILF in left TLE patients for MK, RK, AK, AWF, and MD. A comparable pattern was observed in left Unc for the left lesional TLE patients, with significant changes observed closer to the temporopolar cortex area in MD ($p < 0.005$) and MK, RK, AK, and AWF ($p < 0.05$). For illustrative purposes, the corresponding *p*-values for the microstructural alterations based on MK were mapped along the respective 3D renderings of the fiber bundles (Fig. 3C). As such, it can be observed that MK for the left ILF ($p < 0.005$) and left Unc ($p < 0.05$) from left TLE patients differ most near temporopolar segments of the bundles (i.e., proximal to the left temporopolar cortex). For the ipsilateral temporal lobe in right TLE patients, only weak (i.e., non-significant) differences were detected ipsilateral to seizure focus for the right lesional TLE group based on RK, AWF and MK. Furthermore, exploration of WM bundle profiles within the contralateral side did not reveal significant differences compared to controls for both lesioned and non-lesioned patients (see Supplementary Fig. S1). As such, these will not be considered further in the remainder.

Following multiple comparison corrections, for non-lesional TLE

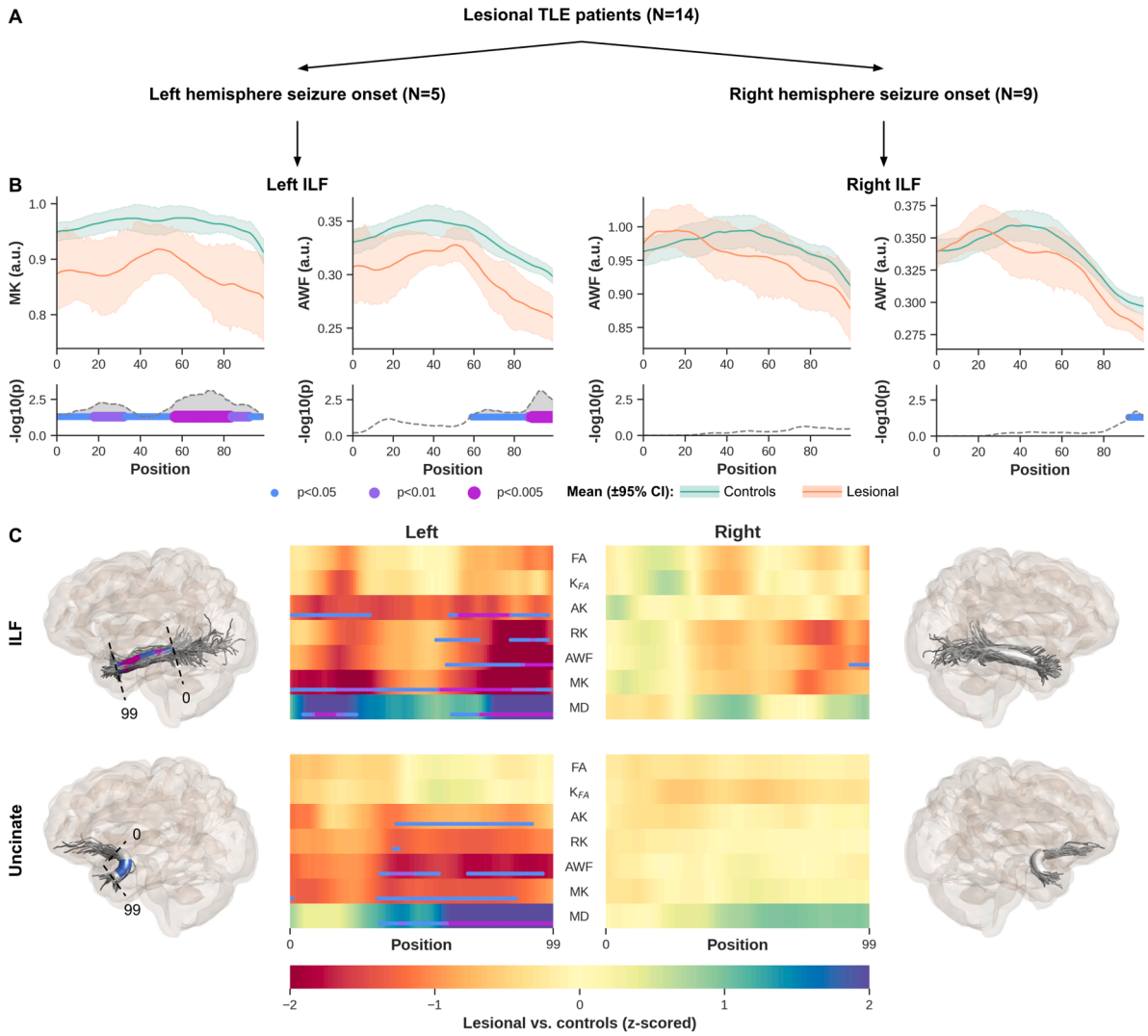

Fig. 3. Left lesional TLE patients' MK, AK, RK, AWK and MD along ILF and Unc demonstrate significant difference relative to controls. Showing only MK and AWF profiles for left and right ILF in lesional left and right TLE patients, respectively (**B**, top row) and corresponding *p*-values corrected for multiple comparisons using FWE, age, and sex (**B**, bottom row). The line and error bars represent the mean and 95% confidence interval, respectively (**B**, top row). To visualize the profile differences at corresponding anatomical locations along the bundles (0–99), the *p*-values for MK are rendered onto the respective fiber bundles (**C**). Showing here on the far left for left ILF (**C**, top row) and Unc (**C**, bottom row). Similarly the right ILF and Unc are shown on the far right **C** top and bottom, respectively. Heat maps show z-scores for all DKI derived maps, for ILF and Unc (**C**). Note that only results from the ipsilateral epileptogenic temporal lobe are shown for each bundle.

patients, no significant differences were observed ipsilateral to the seizure focus (i.e., right/left ILF and Unc in right/left non-lesional TLE, as confirmed with EEG) (Fig. 4). However, indicators of possible changes (i.e., slight differences in z-scores) along the WM bundles were mostly found at their most temporopolar parts in left non-lesional TLE subjects (Fig. 4C), similar to what was observed with the lesional left TLE group (Fig. 3C).

The profiles calculated from the distance maps (i.e., distance from WM voxel to WM-GM boundary, Fig. 5A) from the lesional and non-lesional TLE patient groups and the controls indicate that DKI quantitative sampling occurred exclusively within the WM (i.e., negative distance, Fig. 5B, top row). One thing to note however, is the difference in the mean distance profiles from the WM to the WM-GM interface observed between the patient groups and the controls shown in Fig. 5B. This is also demonstrated on the heat maps (Fig. 5C), in particular ipsilateral to seizure focus ILF and Unc (left lesional TLE) and ipsilateral to seizure focus ILF in left non-lesional TLE and Unc for the right non-lesional TLE group.

3.2. Characterization of white matter DKI profiles

Characterization of the DKI quantitative profiles showed possible differences between the two bundles (ILF and Unc), as shown in Fig. 6. To demonstrate the distribution of the average of the diffusion kurtosis along all diffusion directions (Steven et al., 2014), we show MK and AWF only, the latter as a measure of possible changes in axonal density. A more subtle and variable difference is observed between the patient groups compared to controls' profile as depicted in their skewness, kurtosis, mean(y), and mean(x) distributions. However, in both lesional and non-lesional TLE groups, the SD for the two WM bundles MK (Fig. 6B) and AWF (Fig. 6C) values show consistent dissimilarity compared to controls.

3.3. White matter correlational analyses

When combining the DTI metrics estimated with DKI (i.e., MK + MD and Kfa + FA), we observed significant ($p < 0.05$) differences between the two patients groups (i.e., lesional TLE vs non-lesional TLE) at the

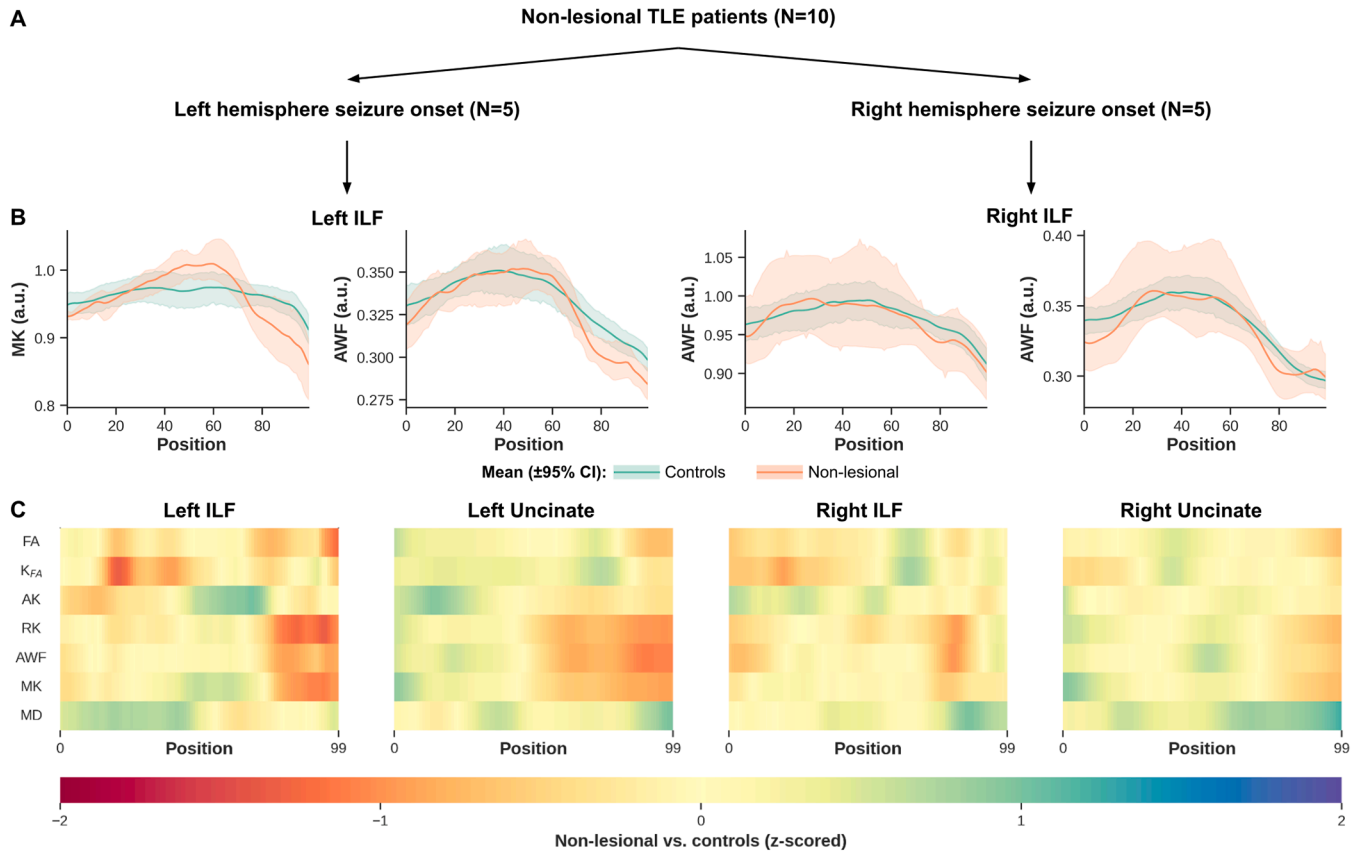

Fig. 4. Non-lesional TLE patients show potential (but non-significant) differences towards temporal pole in their MK, RK and AWF ILF and Unc measurements, relative to controls. Plots show only ILF MK and AWF profiles for left and right ILF in non-lesional left and right TLE patients, respectively (**B**, top row). The line and error bars represent the mean and 95% confidence interval, respectively (**B**, top row). The heat maps show z-scores for all DKI maps including DTI MD and FA estimated with DKI, for ILF and Unc (**C**). Note that only results from the ipsilateral epileptogenic temporal lobe are shown for each bundle.

temporopolar segment (i.e., points 80–99) of the WM bundles within the ipsilateral temporal lobe in left TLE patients (Fig. 7A, right panels). Higher, but not significant z-scores were also observed with MK + MD in ILF and Unc from the left epileptogenic temporal lobe in left lesional TLE patients, compared to Kfa + FA (Fig. 7A, right panels). We also observed a weak trend (i.e., higher variability) with MK + MD in the temporopolar ILF with increase in epilepsy duration as shown in (Fig. S2A).

No significant changes were detected between patient groups and WM bundles when averaging across their temporopolar segment. Nevertheless, in line with the observations for the temporopolar portions of the bundles (i.e., close to temporopolar area), the strongest effects were observed ipsilateral to the seizure focus in left TLE patients' data. Here, lesional TLE patients were characterized by the largest differences, driven primarily by the MK + MD parameters (Fig. 7B, right panels). A more comparable difference was noticed in the ipsilateral temporal lobe between the right lesional and non-lesional TLE patient groups' MK + MD measurements (Fig. 7B, left panels). Based on visual judgment, the DKI combined quantitative values show a pattern of increased differences with persisting seizure in patients as shown in Fig. S2B.

It was noticed that more distinct changes were seen with MK + MD ipsilateral to seizure origin in both lesional and non-lesional left TLE patients. As demonstrated in the Fig. 3A, left panels for the bundles' temporopolar segment (locations 80–99) and the non-temporopolar segments, locations 0–79 (Fig. 3B, left panels).

3.4. Tract-based cortical analysis

We observed consistently strong differences at the temporopolar cortex tissue transition area (i.e., superficial WM towards WM-GM) between the controls and lesional TLE group (Fig. 8B, top row) for the MK, RK, and AWF maps. In the non-lesional TLE group, we also see notable DKI differences, except for MD. In general, z-scores gradually approach zero while moving towards the pial surface. For both patient groups, negligible differences were observed near the RMF region (Fig. 8B, bottom row).

4. Discussion

In this study, we combined the anatomically constrained tractography (ACT) using multishell constrained spherical deconvolution (CSD) (see methods section 2.4) with DKI to compare diffusional properties along (i) the ILF and Uncinate, two major WM fiber bundles connecting the temporal pole with other cortical regions, as well as (ii) the WM to the transition area of the temporal pole, between healthy controls and TLE patients. Most importantly, we found prominent diffusion profile differences closer to the temporopolar portions of both bundles within the side ipsilateral to the epileptogenic temporal lobe. In addition, diffusion anomalies were detected within the temporal pole cortex ipsilateral to the epileptogenic temporal lobe and were more pronounced in the DKI measurements of the TP compared to the reference RMF. This is the first study to combine ACT using multishell CSD to overcome limitations imposed by complex fiber configurations (e.g., crossing fibers) with AFQ for tract profiling and DKI to characterize tissue microstructure, taking into account non-Gaussian diffusion behavior. Furthermore, depth-dependent DKI measurements were extracted to highlight possible diffusion abnormalities from superficial WM towards the pial surface of the TP, a region for which its role in TLE

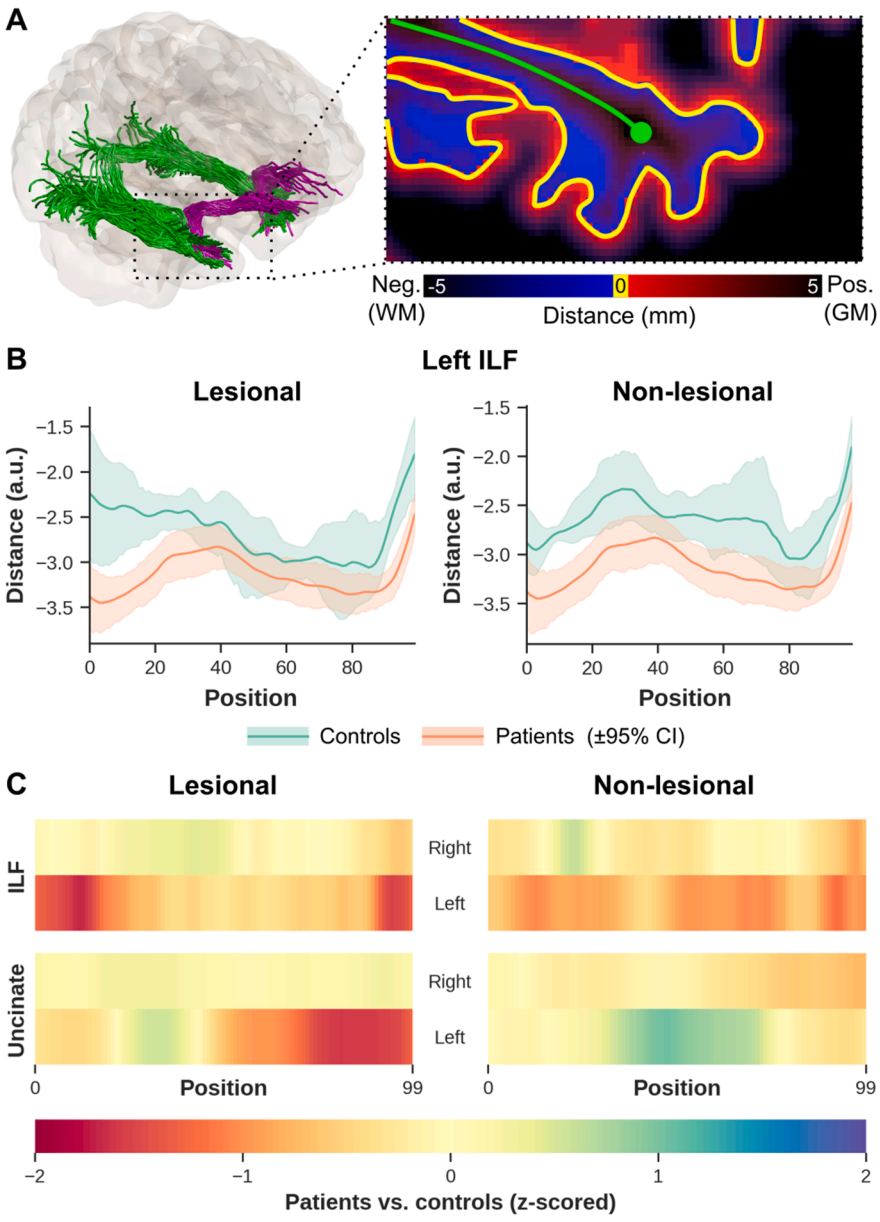

Fig. 5. WM bundle sampling analysis show variability in the mean distance between patients and controls. Example distance map with bright blue (i.e., within WM) and red (within GM) indicating sampling close to the WM-GM interface. The green line indicates the WM fiber bundle centerline (**A**). WM-GM boundary distance profiles from ipsilateral left temporal lobe ILF (left ILF from left lesional and non-lesional TLE) (**B**). The orange profiles show results for lesional (**B**, left) and non-lesional TLE patients (**B,** right). The heat maps show z-scores from the distance profiles for ipsilateral left and right temporal lobe ILF (**C**, top row) and for ipsilateral left and right temporal lobe Unc (**C**, bottom row). (For interpretation of the references to color in this figure legend, the reader is referred to the web version of this article.)

is not well understood (Abel et al., 2018).

4.1. White matter quantitative profiling

Based on the diffusion profiles dissimilarities towards the temporopolar segments of the bundles, more prominent (i.e., statistically significant) differences are observable for the ipsilateral epileptogenic temporal lobe across the left lesional TLE patients, in particular with regards to MK, RK, AK (i.e., decrease), and MD (increase) indicating breakdown of the underlying microstructure, such as alteration in axonal and myelin integrity (Bonilha et al., 2015; Rodríguez-Cruces and Concha, 2015). These findings are in line with a previous study that looked at DKI- and DTI-based metrics along specific WM tracts of left TLE subjects (Glenn et al., 2016). Moreover, as a surrogate marker for axonal density, the decrease in AWF showed potential axonal degradation ipsilateral to the epileptogenic temporal lobe in left lesional TLE patients, which has been a common finding in TLE patients with MTS (Blümcke et al., 2013; Khan et al., 2014; Rodríguez-Cruces and Concha, 2015). We also observed a decrease in DKI parameters and an increase in DKI-based MD towards left TP in both of the bundles ipsilateral to seizure focus in the non-lesional TLE group, however these differences did not reach the significance threshold. We think this could be due to the small sample size of the non-lesional MRI cohort that precluded statistical significance. And also the extratemporal network involvement, that has previously been found in the non-leisional MRI group (Muhlhofer et al., 2017), might have limited us reaching the significant threshold in the bundles (ILF and Unc). Furthermore, although complementary findings to MK, RK, AWK and MD were seen for FA and Kfa, no significant differences were observed. This could be attributed to the fact that (i) FA and Kfa are still influenced by complex fiber configuration reducing their sensitivity to the underlying microstructure (Hansen, 2019), and/or (ii) in contrast to the FA findings in previous studies (Kreilkamp et al., 2017; Labate et al., 2015), we think our approach of quantifying diffusion measurements at specific points along the bundles, rather than just taking an average across ROI, could have contributed to the difference between our study and their analysis. The differences in diffusion abnormalities between the left and right TLE patients, as categorized by seizure onset zone, agrees with a previous voxel-based

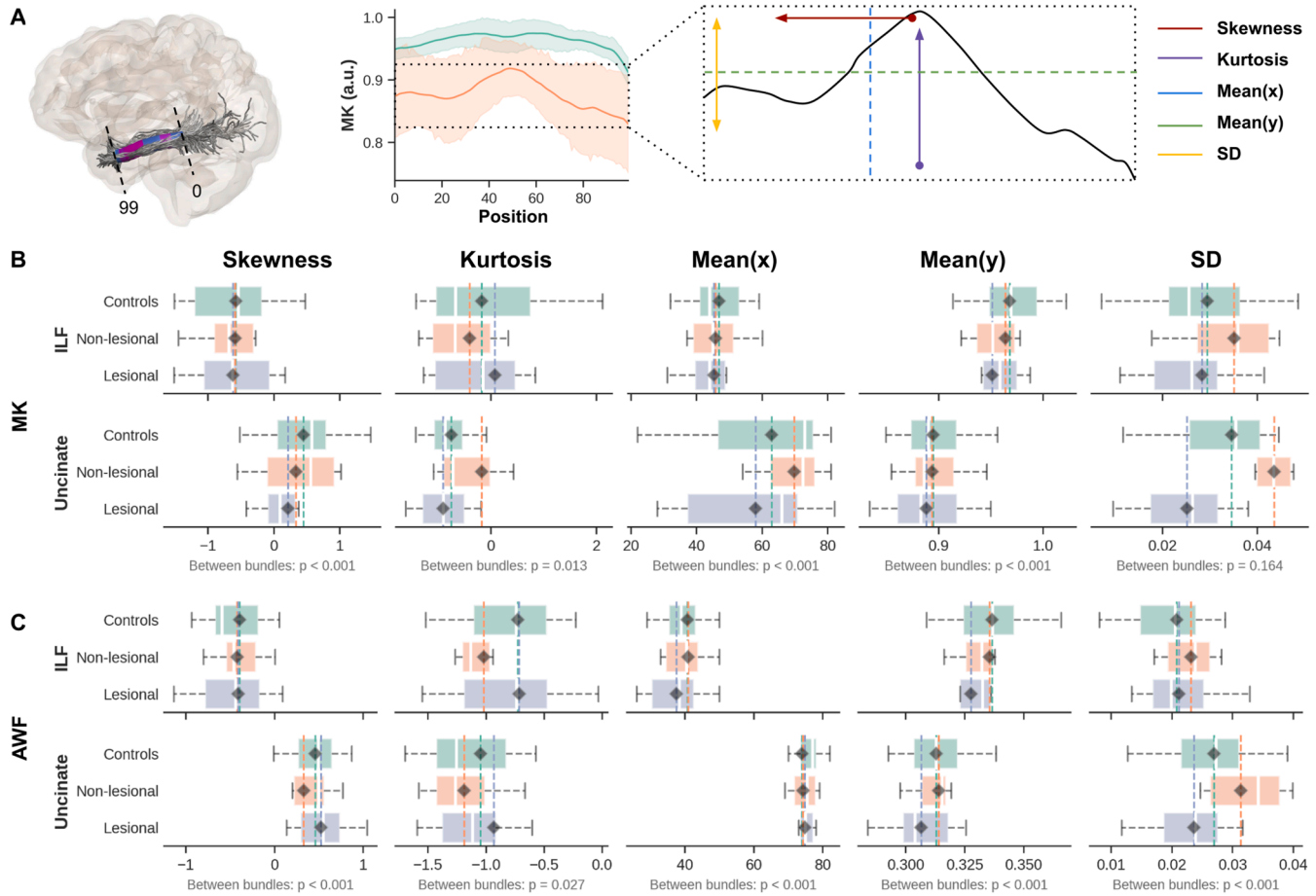

Fig. 6. Characterization of DKI quantitative profiles demonstrate consistent standard deviation (SD) variability across ILF and Unc MK and AWF quantitative maps. The diagram in (**A**) demonstrates the process for deriving profile features (see also methods section) for MK (**B**) and AWF (**C**) per group (y-axis, i.e., lesional TLE in blue, non-lesional TLE in orange, and controls in green). The x-axes are separated with respect to the first four statistical moments; skewness, kurtosis, mean(x) — mean in the x-direction, mean(y) — mean in the y-direction, and the standard deviation (SD) in the rightmost column. Only ipsilateral temporal lobe results from left TLE patients are shown, as these appeared most affected based on the tract profiles. (For interpretation of the references to color in this figure legend, the reader is referred to the web version of this article.)

study demonstrating widespread and prominent DTI abnormalities in patients with MTS and left hemispheric onset, while right non-lesional TLE patients exhibited no detectable changes (Shon et al., 2010). The observed variability in diffusion anomalies could be related to the inherent distinction in different TLE types and their pathological effects on the temporal pole and the connected WM, particularly in left versus right TLE patients (Besson et al., 2014; Keller et al., 2002). In addition, the findings in this study agree very closely with the accumulating evidence of left TLE showing a more distributed, bilateral pattern of structural changes compared to patients with right TLE (Bonilha et al., 2007; Kemmotsu et al., 2011). White matter and cortical disruption have been also reported in a number of previous studies, with left TLE exhibiting more widespread atrophy, beyond the epileptic temporal lobe compared to right TLE group (Ahmadi et al., 2009; Kemmotsu et al., 2011). However, the mechanism underlying the differences in left verse right TLE abnormalities is still unclear. Several studies suggest that, the discrepancy between left and right TLE may have stemmed from the slower maturity of left hemisphere compared to the right side making it vulnerable to early insults from febrile and early-onset seizures (Corballis and Morgan, 1978; Kemmotsu et al., 2011). The significant increase in MD and decrease in MK and RK noticed in left lesional TLE group in our study support the idea of widened extra-axonal space (i.e., allowing increase in free water) due to disruption of myelin sheaths and axonal membranes as well as decreased fiber density (Winston et al., 2020). Previous histology and DTI correlation work have shown that increase in FA and MD were due to reduction of axonal density and alterations in the myelin architecture within the left temporal lobe (Concha et al., 2010; Deleo et al., 2018), including a marked temporal pole connectivity reduction in left TLE group observed by (Besson et al., 2014). Furthermore, reduction in smaller caliber axons and presence of histology features such as glioses may also play a role in diffusion anomalies (Deleo et al., 2018).

This suggests that DKI could serve as a complementary approach to detect subtle changes in the WM fiber bundles connected to the TP. In addition, the observed reduction in the distance of the patients' WM fiber bundles to the WM-GM boundary could be attributed to the presence of ectopic WM neurons (i.e., WM neurons in abnormal locations, mostly found in the subcortical region) which increase in density in brain specimens of TLE patients compared to controls (Emery et al., 1997). Previous voxel- and region-based studies (Bonilha et al., 2015; Shon et al., 2010) observed abnormalities along the WM fiber bundles in the ipsilateral temporal tracts. Here we demonstrate that DKI, combined with AFQ based on anatomically-constrained tracking, has the ability to identify abnormalities at specific locations along WM fiber bundles, in this case the ILF and Unc, both connected to the temporal pole, thus providing granular details of their microstructure composition. Such information, especially before surgery in TLE, could be used to guide the procedure by more completely identifying the seizure onset zone and the region(s) to be resected, potentially resulting in improved outcomes. However, although the current findings demonstrate DKI's potential to

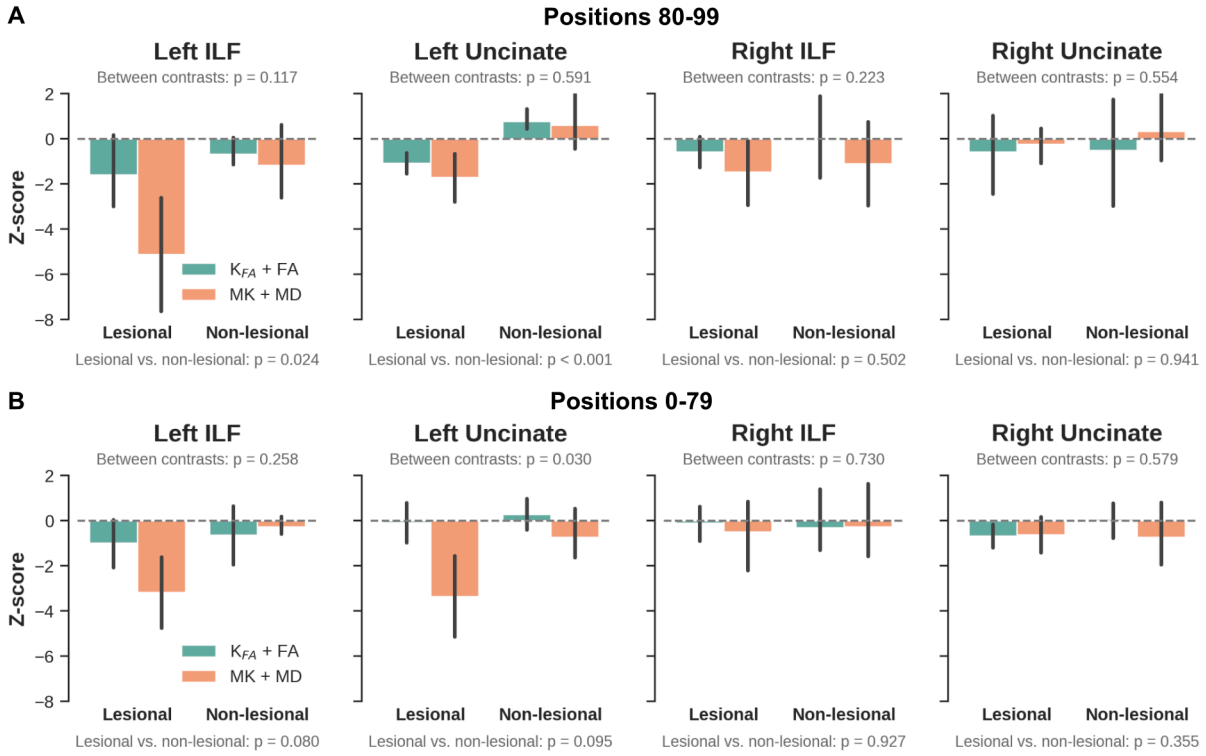

Fig. 7. Combined DKI parameter analysis finds left TLE with stronger and complementary differences along the bundle length in MK + MD and Kfa + FA, respectively. The bar plots (top row, A) show z-scores (Kfa + FA, green) and (MK + MD, orange) for lesional TLE and non-lesional TLE patients vs controls calculated within the ipsilateral temporal lobe for ILF (left panels) and Unc using values extracted from sampling points (80–99). **B**, combined DKI parameter analysis, values extracted from sampling points (0–79). Between contrast (i.e., MK + MD vs Kfa + FA) and between patient groups *p*-values (corrected for age and sex) are shown in gray. Note, the points 0–79 and 80–99 were selected to obtain bundle segments more distal and proximal to the temporal pole, respectively. (For interpretation of the references to color in this figure legend, the reader is referred to the web version of this article.)

measure diffusion in patients, it strongly motivates further evaluation with a larger patient cohort.

4.2. Characterization of white matter DKI profiles

Tract profile analysis of the MK and AWF values along WM bundles (i.e., between sampling points 0–99), indicated that ILF and Unc ipsilateral to seizure focus have a wider SD in the non-lesional TLE group (more pronounced in Unc). Here, SD represents the variation along the y-axis of the profiles, implying that MK and AWF appear to vary more along points 0–99 for the non-lesional TLE, but are more 'flat' for the lesional TLE patients, compared to controls. This observation could correspond to the considerable evidence of dispersed diffusion abnormalities observed in non-lesional TLE patients compared to those with TLE patients having radiological evidence of MTS (i.e., lesional TLE) (Keller et al., 2013; Rodríguez-Cruces and Concha, 2015). In addition, a smaller SD of the AWF data for the lesional TLE patients could also suggest diffusion anomalies related to degradation of spatial specificity of microstructural properties along the WM pathways compared to the more variable changes exhibited with non-lesional TLE patients. Furthermore, between the bundles, Unc shows greater deviations than ILF in the non-lesional TLE patients, in concordance to a previous tract base study, which found a significant reduction in the Unc, that was more pronounced in the anterior temporal lobe (Glenn et al., 2016). These differences observed in the DKI parameter distribution, specifically SD, agree with the WM profiling analysis indicating potential diffusional changes due to patterns of neuronal loss and gliosis, particularly observed in patients with MTS (Blümcke et al., 2013).

4.3. White matter correlational analysis

The complementary properties of the MK and MD (i.e., restricted vs free diffusion) parameters were utilized by combining their respective z-scores. In agreement with the WM findings, a significant difference at the temporopolar portion of the bundles between the two patient types (lesional TLE vs non-lesional TLE) was observed. MK + MD demonstrated potential microstructural changes in the ipsilateral epileptogenic temporal lobe, where left lesional TLE showed stronger differences compared to left non-lesional TLE group, especially towards the temporopolar segments of the two fiber bundles (i.e., from sampling point 80 right to the end point 99). Similar, but milder diffusional changes were reflected in the MK + MD values within the non-temporopolar segments (i.e., points 0–79) of the ILF and Unc, with noticeable differences for left TLE (i.e., left lesional TLE and non-lesional TLE) patients compared to controls. Although, these differences did not appear statistically significant, our findings go along with a previous study that demonstrated a centrifugal decrease of DTI-based abnormalities as WM networks extend away from the epileptogenic temporal lobe (Concha et al., 2012; Rodríguez-Cruces and Concha, 2015). Furthermore, there was a relationship between the MK + MD measurements and disease duration in the two patient groups (lesional TLE and non-lesional TLE). The detected progressive diffusion anomalies suggest gradual microstructural changes due to persistent seizure activities (Keller et al., 2012). This pattern was also noted in a DTI-base study, with MD strongly correlating with disease duration (Chiang et al., 2016). Although MK + MD showed clear differences compared to Kfa + FA, there were no significant differences between these combined DKI parameters (i.e., MK + MD vs Kfa + FA). Nevertheless, since MK and MD are average measurements along all diffusion weighting directions in restricted and free diffusion environments respectively, we expected MK + MD to

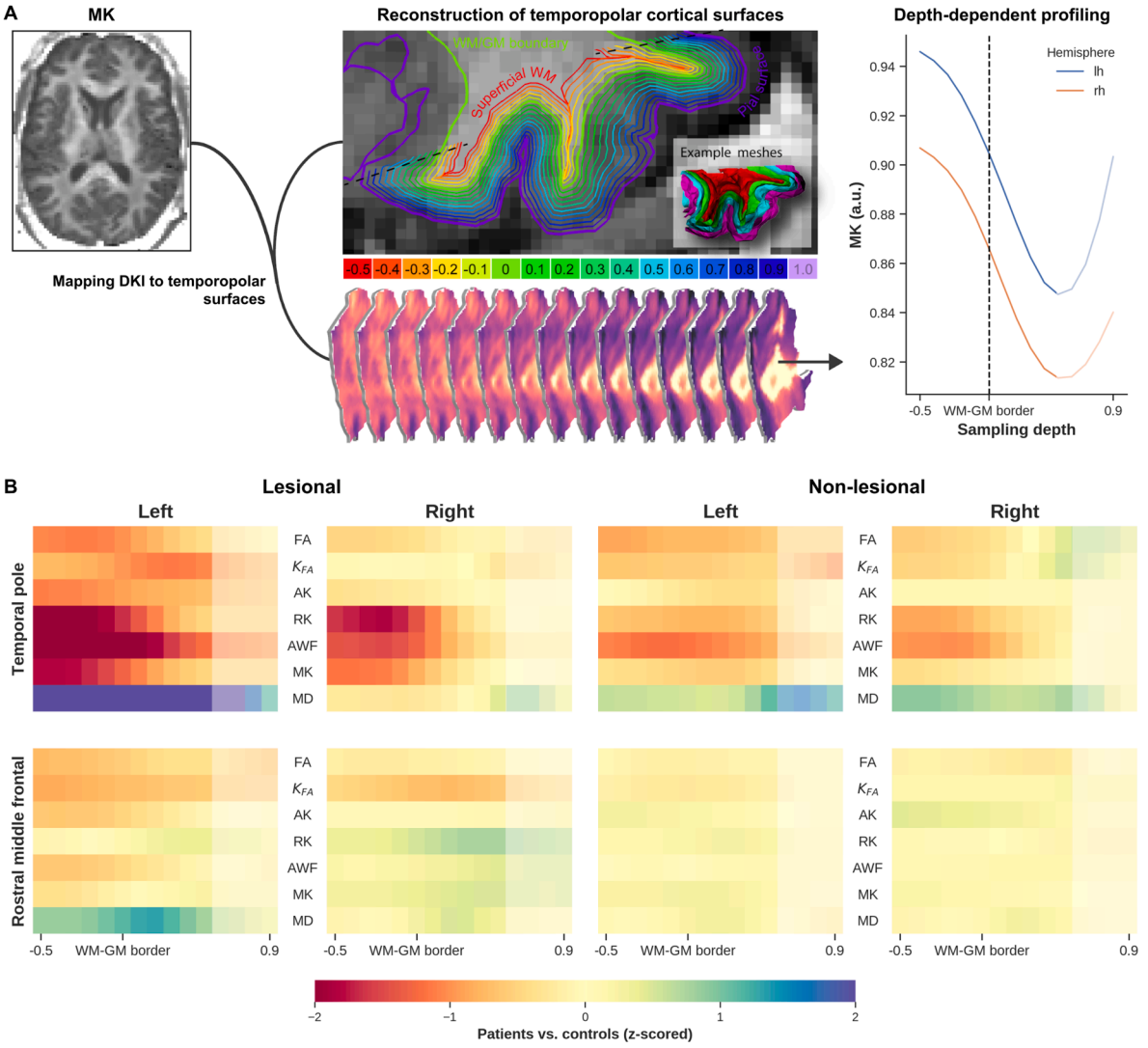

Fig. 8. Tract-based cortical analyses indicates potential microstructural anomalies in the temporopolar cortex compared to an extratemporal region (rostral middle temporal). The general workflow for the cortical diffusion profiling is shown in (**A**). The DKI quantitative values (e.g. MK, left **A**) are projected onto the temporopolar surfaces at varying depths, starting from the superficial WM (middle **A**, red) towards the pial surface (purple). Finally, quantitative measurements of the temporopolar cortex microstructure are extracted as depth-dependent profiles (right **A**) (see also methods section). Comparison of cortical microstructure between patients and controls is shown in (**B**). Each heatmap shows z-scores for all DKI parameters extracted from the superficial WM (i.e., −0.5) towards the pial surface (0.9). The top row shows lesional TLE patients vs controls (left columns) and non-lesional TLE patients vs controls (right columns) calculated within the temporopolar cortex ipsilateral to the epileptogenic temporal lobe, similarly the bottom row presents rostral middle temporal. Note: The increased MK values towards the pial surface (**A**, line plot) show a possibility of cerebrospinal fluid (CSF) influence (depths 0.5 to 1.0, indicated with semi-transparent color), so care should be taken when interpreting these results. (For interpretation of the references to color in this figure legend, the reader is referred to the web version of this article.)

provide a comprehensive characterization of diffusion properties depicting tissue integrity. On the other hand, FA depicts the preferred direction of diffusion and can reduce drastically in areas of crossing fibers or often in regions of coherent WM (Hansen, 2019). Therefore by combining FA and Kfa, complementary information regarding tissue microstructure could be derived (Hansen, 2019).

4.4. Tract-based cortical analysis

The present findings indicate that MK and RK can detect microstructure anomalies within the temporopolar cortex in lesional TLE, and to some extent within the non-lesional TLE patients compared to a reference region (i.e., RMF). Although TLE appears to be characterized by a network of abnormalities (Bonilha et al., 2015), we expected RMF to have a minimal association with the temporopolar cortex changes due to seizure activities. Besides the observations related to MK and RK, the changes in AWF indicate potential neuronal loss. This could be due to seizure activity originating either at the temporopolar cortex or the medial temporal lobe structures (e.g. hippocampus) (Chabardès et al., 2005). These findings support previous work which detected neurons and dendritic changes in the temporopolar cortex in TLE patients (Winston et al., 2020). Parallel to this study and in support of our findings, several earlier imaging- and histology-based studies have also identified a reduction in neuronal density and gliosis within the superficial WM and temporopolar cortex (Bonilha et al., 2010; Kuzniecky et al., 1987). Furthermore, the WM-GM boundary diffusion anomalies could be related to the blurring of this area, commonly attributed to various causes (e.g. developmental cortical abnormalities, gliosis, or myelin alterations) (Emery et al., 1997; Garbelli et al., 2012). Based on the current results, DKI could serve as a complementary approach to detect subtle microstructural alterations within the temporopolar cortex. Understanding the role of TP in TLE is important to inform

resection, which could help to minimize seizure recurrence due to insufficient resection (Harroud et al., 2012).

4.5. Limitations

The diffusion anomalies along the WM fiber bundles that connect the TP and temporopolar cortex to the rest of the brain indicate DKI's ability to quantify subtle alterations of tissue microstructure in TLE patients. However, future work may include a larger cohort of (lesional TLE and non-lesional TLE) patients to validate these findings. For example, a power analysis (with alpha = 0.05, power = 0.80) based on a maximum Cohen's d effect size of 0.78 (i.e., *T*-statistic = 1.96) for the non-lesioned, left ILF patients (N = 5), suggest that a minimum sample size of 27 patients is required to establish the observed differences in this particular group. This was calculated following the implementation within pingouin's *power_ttest* function. The spatial resolution (2 mm isotropic) of the DWI used in this study is approximately equivalent to the cortical thickness (Hutton et al., 2008). Therefore, the current findings could still be affected by partial volume effects near CSF. As such, data closer to the pial surface (i.e., sampling depth greater than 0.5) were not taken into consideration. Nevertheless, as we were particularly interested in the WM-GM transition area, the current TCA is still valid to reveal trends in terms of microstructural differences in the TLE patients. Moreover, statistical results were corrected for age and sex to minimize their influence on the patient vs control differences. However, age- and sex-matched samples could avoid any residual differences in diffusion characteristics due to aging or gender (Pal et al., 2011; Wu et al., 2011). Besides, only side of seizure onset was considered here for patients' stratification while other factors like lesion type (e.g., hippocampal sclerosis vs neuroepithelial tumors) might provide relevant information as well. Furthermore, our patient cohort might include patients with possible involvement of contralateral side (e.g., patient ID5), this could have added to the variability observed.

5. Conclusions

The current study demonstrated that the combination of ACT multi-shell tracking, AFQ, and DKI could serve as a complementary approach to detect subtle microstructural alterations within the temporopolar segments of the two association WM fiber bundles connected to the temporal pole. In addition, depth-dependent DKI measurements could aid in uncovering diffusion abnormalities in the temporopolar cortex. Furthermore, since DKI acquisition with the desired precision has been shown to be clinically feasible (Kasa et al., 2021), the methods developed in this study could be easily implemented in a clinical workflow. Finally, while the study was based on a limited patient cohort it provides solid preliminary data upon which to base a more comprehensive investigation. Identification of anomalies along the WM bundles segments and specific depths within the temporopolar cortex before surgery could help inform the planning of selective resection to improve outcome in TLE patients.

CRediT authorship contribution statement

Loxlan W. Kasa: Conceptualization, Methodology, Software, Formal analysis, Writing – original draft, Writing – review & editing, Project administration. **Terry Peters:** Funding acquisition, Supervision, Writing – review & editing. **Seyed M. Mirsattari:** Data curation, Writing – review & editing. **Michael T. Jurkiewicz:** Data curation, Writing – review & editing. **Ali R. Khan:** Conceptualization, Funding acquisition, Supervision, Writing – review & editing. **Roy A.M Haast:** Methodology, Software, Formal analysis, Writing – review & editing.

Declaration of Competing Interest

The authors declare that they have no known competing financial interests or personal relationships that could have appeared to influence the work reported in this paper.

Data availability

Data will be made available on request.

Acknowledgement

We would like to thank the patients and control participants who agreed to take part in this study. This work was supported by Canadian Institutes of Health Research (CIHR) Foundation (grant number 333550), Natural Sciences and Engineering Research Council (NSERC) Discovery (grant number RGPIN-2015-06639), Canada Research Chairs (grant number 950-231964), Canada Foundation for Innovation (CFI) John R. Evans Leaders Fund project number 37427, the Canada First Research Excellence Fund, Brain Canada, and the Ontario Brain Institute Epilepsy Program (EpLink). Author R.A.M.H was supported by a BrainsCAN postdoctoral fellowship for this work.

Appendix A. Supplementary data

Supplementary data to this article can be found online at https://doi.org/10.1016/j.nicl.2022.103201.

References

Abel, T.J., Woodroffe, R.W., Nourski, K.V., Moritani, T., Capizzano, A.A., Kirby, P., Kawasaki, H., Howard, M., Werz, M.A., 2018. Role of the temporal pole in temporal lobe epilepsy seizure networks: an intracranial electrode investigation. J. Neurosurg. 129, 165–173. https://doi.org/10.3171/2017.3.JNS162821.

Ahmadi, M.E., Hagler Jr, D.J., McDonald, C.R., Tecoma, E.S., Iragui, V.J., Dale, A.M., Halgren, E., 2009. Side matters: diffusion tensor imaging tractography in left and right temporal lobe epilepsy. AJNR Am. J. Neuroradiol. 30, 1740–1747. https://doi.org/10.3174/ajnr.A1650.

Amunts, K., Schleicher, A., Bürgel, U., Mohlberg, H., Uylings, H.B., Zilles, K., 1999. Broca's region revisited: cytoarchitecture and intersubject variability. J. Comp. Neurol. 412, 319–341. https://doi.org/10.1002/(sici)1096-9861(19990920)412:2<319::aid-cne10>3.0.co;2-7.

Andersson, J.L.R., Skare, S., Ashburner, J., 2003. How to correct susceptibility distortions in spin-echo echo-planar images: application to diffusion tensor imaging. Neuroimage 20, 870–888. https://doi.org/10.1016/S1053-8119(03)00336-7.

Andersson, J.L.R., Sotiropoulos, S.N., 2016. An integrated approach to correction for off-resonance effects and subject movement in diffusion MR imaging. Neuroimage 125, 1063–1078. https://doi.org/10.1016/j.neuroimage.2015.10.019.

Bartolomei, F., Lagarde, S., Wendling, F., McGonigal, A., Jirsa, V., Guye, M., Bénar, C., 2017. Defining epileptogenic networks: Contribution of SEEG and signal analysis. Epilepsia 58, 1131–1147. https://doi.org/10.1111/epi.13791.

Berkovic, S.F., McIntosh, A.M., Kalnins, R.M., Jackson, G.D., Fabinyi, G.C., Brazenor, G. A., Bladin, P.F., Hopper, J.L., 1995. Preoperative MRI predicts outcome of temporal lobectomy: an actuarial analysis. Neurology 45, 1358–1363. https://doi.org/10.1212/wnl.45.7.1358.

Besson, P., Dinkelacker, V., Valabregue, R., Thivard, L., Leclerc, X., Baulac, M., Sammler, D., Colliot, O., Lehéricy, S., Samson, S., Dupont, S., 2014. Structural connectivity differences in left and right temporal lobe epilepsy. Neuroimage 100, 135–144. https://doi.org/10.1016/j.neuroimage.2014.04.071.

Blümcke, I., Thom, M., Aronica, E., Armstrong, D.D., Bartolomei, F., Bernasconi, A., Bernasconi, N., Bien, C.G., Cendes, F., Coras, R., Cross, J.H., Jacques, T.S., Kahane, P., Mathern, G.W., Miyata, H., Moshé, S.L., Oz, B., Özkara, Ç., Perucca, E., Sisodiya, S., Wiebe, S., Spreafico, R., 2013. International consensus classification of hippocampal sclerosis in temporal lobe epilepsy: a Task Force report from the ILAE Commission on Diagnostic Methods. Epilepsia 54, 1315–1329. https://doi.org/10.1111/epi.12220.

Bonilha, L., Rorden, C., Halford, J.J., Eckert, M., Appenzeller, S., Cendes, F., Li, L.M., 2007. Asymmetrical extra-hippocampal grey matter loss related to hippocampal atrophy in patients with medial temporal lobe epilepsy. J. Neurol. Neurosurg. Psychiatry 78, 286–294. https://doi.org/10.1136/jnnp.2006.103994.

Bonilha, L., Edwards, J.C., Kinsman, S.L., Morgan, P.S., Fridriksson, J., Rorden, C., Rumboldt, Z., Roberts, D.R., Eckert, M.A., Halford, J.J., 2010. Extrahippocampal gray matter loss and hippocampal deafferentation in patients with temporal lobe epilepsy. Epilepsia 51, 519–528. https://doi.org/10.1111/j.1528-1167.2009.02506.x.

Bonilha, L., Lee, C.-Y., Jensen, J.H., Tabesh, A., Spampinato, M.V., Edwards, J.C., Breedlove, J., Helpern, J.A., 2015. Altered microstructure in temporal lobe epilepsy: a diffusional kurtosis imaging study. AJNR Am. J. Neuroradiol. 36, 719–724. https://doi.org/10.3174/ajnr.A4185.

Catani, M., Thiebaut de Schotten, M., 2008. A diffusion tensor imaging tractography atlas for virtual in vivo dissections. Cortex 44, 1105–1132. https://doi.org/10.1016/j.cortex.2008.05.004.

Chabardès, S., Kahane, P., Minotti, L., Tassi, L., Grand, S., Hoffmann, D., Benabid, A.L., 2005. The temporopolar cortex plays a pivotal role in temporal lobe seizures. Brain 128, 1818–1831. https://doi.org/10.1093/brain/awh512.

Chiang, S., Levin, H.S., Wilde, E., Haneef, Z., 2016. White matter structural connectivity changes correlate with epilepsy duration in temporal lobe epilepsy. Epilepsy Res. 120, 37–46. https://doi.org/10.1016/j.eplepsyres.2015.12.002.

Concha, L., Kim, H., Bernasconi, A., Bernhardt, B.C., Bernasconi, N., 2012. Spatial patterns of water diffusion along white matter tracts in temporal lobe epilepsy. Neurology 79, 455–462. https://doi.org/10.1212/WNL.0b013e31826170b6.

Corballis, M.C., Morgan, M.J., 1978. On the biological basis of human laterality: I. Evidence for a maturational left–right gradient. Behav Brain Sci 1 (2), 261–269.

DeKraker, J., Lau, J.C., Ferko, K.M., Khan, A.R., Köhler, S., 2020. Hippocampal subfields revealed through unfolding and unsupervised clustering of laminar and morphological features in 3D BigBrain. Neuroimage 206, 116328. https://doi.org/10.1016/j.neuroimage.2019.116328.

Deleo, F., Thom, M., Concha, L., Bernasconi, A., Bernhardt, B.C., Bernasconi, N., 2018. Histological and MRI markers of white matter damage in focal epilepsy. Epilepsy Res. 140, 29–38. https://doi.org/10.1016/j.eplepsyres.2017.11.010.

Dhollander, T., Connelly, A., 2016. ISMRM Workshop on Breaking the Barriers of Diffusion MRI.

Emery, J.A., Roper, S.N., Rojiani, A.M., 1997. White matter neuronal heterotopia in temporal lobe epilepsy: a morphometric and immunohistochemical study. J. Neuropathol. Exp. Neurol. 56, 1276–1282. https://doi.org/10.1097/00005072-199712000-00002.

Engel Jr, J., 2006. Report of the ILAE classification core group. Epilepsia 47, 1558–1568. https://doi.org/10.1111/j.1528-1167.2006.00215.x.

Fieremans, E., Jensen, J.H., Helpern, J.A., 2011. White matter characterization with diffusional kurtosis imaging. Neuroimage 58, 177–188. https://doi.org/10.1016/j.neuroimage.2011.06.006.

Garbelli, R., Milesi, G., Medici, V., Villani, F., Didato, G., Deleo, F., D'Incerti, L., Morbin, M., Mazzoleni, G., Giovagnoli, A.R., Parente, A., Zucca, I., Mastropietro, A., Spreafico, R., 2012. Blurring in patients with temporal lobe epilepsy: clinical, high-field imaging and ultrastructural study. Brain 135, 2337–2349. https://doi.org/10.1093/brain/aws149.

Georgiadis, I., Kapsalaki, E.Z., Fountas, K.N., 2013. Temporal lobe resective surgery for medically intractable epilepsy: a review of complications and side effects. Epilepsy Res. Treat. 2013, 752195. https://doi.org/10.1155/2013/752195.

Glenn, G.R., Jensen, J.H., Helpern, J.A., Spampinato, M.V., Kuzniecky, R., Keller, S.S., Bonilha, L., 2016. Epilepsy-related cytoarchitectonic abnormalities along white matter pathways. J. Neurol. Neurosurg. Psychiatry 87, 930–936. https://doi.org/10.1136/jnnp-2015-312980.

Hansen, B., 2019. An Introduction to Kurtosis Fractional Anisotropy. AJNR Am. J. Neuroradiol. 40, 1638–1641. https://doi.org/10.3174/ajnr.A6235.

Harroud, A., Bouthillier, A., Weil, A.G., Nguyen, D.K., 2012. Temporal lobe epilepsy surgery failures: a review. Epilepsy Res. Treat. 2012, 201651. https://doi.org/10.1155/2012/201651.

Horbruegger, M., Loewe, K., Kaufmann, J., Wagner, M., Schippling, S., Pawlitzki, M., Schoenfeld, M.A., 2019. Anatomically constrained tractography facilitates biologically plausible fiber reconstruction of the optic radiation in multiple sclerosis. Neuroimage Clin 22, 101740. https://doi.org/10.1016/j.nicl.2019.101740.

Hua, K., Zhang, J., Wakana, S., Jiang, H., Li, X., Reich, D.S., Calabresi, P.A., Pekar, J.J., van Zijl, P.C.M., Mori, S., 2008. Tract probability maps in stereotaxic spaces: analyses of white matter anatomy and tract-specific quantification. Neuroimage 39, 336–347. https://doi.org/10.1016/j.neuroimage.2007.07.053.

Hutton, C., De Vita, E., Ashburner, J., Deichmann, R., Turner, R., 2008. Voxel-based cortical thickness measurements in MRI. Neuroimage 40, 1701–1710. https://doi.org/10.1016/j.neuroimage.2008.01.027.

Jehi, L., Friedman, D., Carlson, C., Cascino, G., Dewar, S., Elger, C., Engel Jr, J., Knowlton, R., Kuzniecky, R., McIntosh, A., O'Brien, T.J., Spencer, D., Sperling, M.R., Worrell, G., Bingaman, B., Gonzalez-Martinez, J., Doyle, W., French, J., 2015. The evolution of epilepsy surgery between 1991 and 2011 in nine major epilepsy centers across the United States, Germany, and Australia. Epilepsia 56, 1526–1533. https://doi.org/10.1111/epi.13116.

Jensen, J.H., Helpern, J.A., Ramani, A., Lu, H., Kaczynski, K., 2005. Diffusional kurtosis imaging: the quantification of non-gaussian water diffusion by means of magnetic resonance imaging. Magn. Reson. Med. 53, 1432–1440. https://doi.org/10.1002/mrm.20508.

Jeurissen, B., Tournier, J.-D., Dhollander, T., Connelly, A., Sijbers, J., 2014. Multi-tissue constrained spherical deconvolution for improved analysis of multi-shell diffusion MRI data. Neuroimage 103, 411–426. https://doi.org/10.1016/j.neuroimage.2014.07.061.

Kasa, L.W., Haast, R.A.M., Kuehn, T.K., Mushtaha, F.N., Baron, C.A., Peters, T., Khan, A. R., 2021. Evaluating High Spatial Resolution Diffusion Kurtosis Imaging at 3T: Reproducibility and Quality of Fit. J. Magn. Reson. Imaging 53, 1175–1187. https://doi.org/10.1002/jmri.27408.

Keller, S.S., Mackay, C.E., Barrick, T.R., Wieshmann, U.C., Howard, M.A., Roberts, N., 2002. Voxel-based morphometric comparison of hippocampal and extrahippocampal abnormalities in patients with left and right hippocampal atrophy. Neuroimage 16, 23–31. https://doi.org/10.1006/nimg.2001.1072.

Keller, S.S., Schoene-Bake, J.-C., Gerdes, J.S., Weber, B., Deppe, M., Zhan, W., 2012. Concomitant fractional anisotropy and volumetric abnormalities in temporal lobe epilepsy: cross-sectional evidence for progressive neurologic injury. PLoS One 7 (10), e46791. https://doi.org/10.1371/journal.pone.0046791.

Keller, S.S., Ahrens, T., Mohammadi, S., Gerdes, J.S., Möddel, G., Kellinghaus, C., Kugel, H., Weber, B., Ringelstein, E.B., Deppe, M., 2013. Voxel-based statistical analysis of fractional anisotropy and mean diffusivity in patients with unilateral temporal lobe epilepsy of unknown cause. J. Neuroimaging 23, 352–359. https://doi.org/10.1111/j.1552-6569.2011.00673.x.

Kellner, E., Dhital, B., Kiselev, V.G., Reisert, M., 2016. Gibbs-ringing artifact removal based on local subvoxel-shifts. Magn. Reson. Med. 76, 1574–1581. https://doi.org/10.1002/mrm.26054.

Kemmotsu, N., Girard, H.M., Bernhardt, B.C., Bonilha, L., Lin, J.J., Tecoma, E.S., Iragui, V.J., Hagler Jr, D.J., Halgren, E., McDonald, C.R., 2011. MRI analysis in temporal lobe epilepsy: cortical thinning and white matter disruptions are related to side of seizure onset. Epilepsia 52, 2257–2266. https://doi.org/10.1111/j.1528-1167.2011.03278.x.

Khan, A.R., Goubran, M., de Ribaupierre, S., Hammond, R.R., Burneo, J.G., Parrent, A.G., Peters, T.M., 2014. Quantitative relaxometry and diffusion MRI for lateralization in MTS and non-MTS temporal lobe epilepsy. Epilepsy Res. 108, 506–516. https://doi.org/10.1016/j.eplepsyres.2013.12.012.

Kreilkamp, B.A.K., Weber, B., Richardson, M.P., Keller, S.S., 2017. Automated tractography in patients with temporal lobe epilepsy using TRActs Constrained by UnderLying Anatomy (TRACULA). Neuroimage Clin 14, 67–76. https://doi.org/10.1016/j.nicl.2017.01.003.

Kuzniecky, R., de la Sayette, V., Ethier, R., Melanson, D., Andermann, F., Berkovic, S., Robitaille, Y., Olivier, A., Peters, T., Feindel, W., 1987. Magnetic resonance imaging in temporal lobe epilepsy: pathological correlations. Ann. Neurol. 22, 341–347. https://doi.org/10.1002/ana.410220310.

Labate, A., Cherubini, A., Tripepi, G., Mumoli, L., Ferlazzo, E., Aguglia, U., Quattrone, A., Gambardella, A., 2015. White matter abnormalities differentiate severe from benign temporal lobe epilepsy. Epilepsia 56, 1109–1116. https://doi.org/10.1111/epi.13027.

Liu, M., Bernhardt, B.C., Hong, S.-J., Caldairou, B., Bernasconi, A., Bernasconi, N., 2016. The superficial white matter in temporal lobe epilepsy: a key link between structural and functional network disruptions. Brain 139, 2431–2440. https://doi.org/10.1093/brain/aww167.

Lorio, S., Adler, S., Gunny, R., D'Arco, F., Kaden, E., Wagstyl, K., Jacques, T.S., Clark, C. A., Cross, J.H., Baldeweg, T., Carmichael, D.W., 2020. MRI profiling of focal cortical dysplasia using multi-compartment diffusion models. Epilepsia 61, 433–444. https://doi.org/10.1111/epi.16451.

McKinnon, E.T., Fridriksson, J., Basilakos, A., Hickok, G., Hillis, A.E., Spampinato, M.V., Gleichgerrcht, E., Rorden, C., Jensen, J.H., Helpern, J.A., Bonilha, L., 2018. Types of naming errors in chronic post-stroke aphasia are dissociated by dual stream axonal loss. Sci. Rep. 8, 14352. https://doi.org/10.1038/s41598-018-32457-4.

Muhlhofer, W., Tan, Y.-L., Mueller, S.G., Knowlton, R., 2017. MRI-negative temporal lobe epilepsy-What do we know? Epilepsia 58, 727–742. https://doi.org/10.1111/epi.13699.

Pal, D., Trivedi, R., Saksena, S., Yadav, A., Kumar, M., Pandey, C.M., Rathore, R.K.S., Gupta, R.K., 2011. Quantification of age- and gender-related changes in diffusion tensor imaging indices in deep grey matter of the normal human brain. Journal of Clinical Neuroscience 18 (2), 193–196.

Rodríguez-Cruces, R., Concha, L., 2015. White matter in temporal lobe epilepsy: clinico-pathological correlates of water diffusion abnormalities. Quant. Imaging Med. Surg. 5, 264–278. https://doi.org/10.3978/j.issn.2223-4292.2015.02.06.

Shon, Y.-M., Kim, Y.-I., Koo, B.-B., Lee, J.-M., Kim, H.J., Kim, W.J., Ahn, K.J., Yang, D.W., 2010. Group-specific regional white matter abnormality revealed in diffusion tensor imaging of medial temporal lobe epilepsy without hippocampal sclerosis. Epilepsia 51, 529–535. https://doi.org/10.1111/j.1528-1167.2009.02327.x.

Smith, S.M., Jenkinson, M., Woolrich, M.W., Beckmann, C.F., Behrens, T.E.J., Johansen-Berg, H., Bannister, P.R., De Luca, M., Drobnjak, I., Flitney, D.E., Niazy, R.K., Saunders, J., Vickers, J., Zhang, Y., De Stefano, N., Brady, J.M., Matthews, P.M., 2004. Advances in functional and structural MR image analysis and implementation as FSL. S219 Neuroimage 23 (Suppl 1), S208. https://doi.org/10.1016/j.neuroimage.2004.07.051.

Smith, R.E., Tournier, J.-D., Calamante, F., Connelly, A., 2012. Anatomically-constrained tractography: improved diffusion MRI streamlines tractography through effective use of anatomical information. Neuroimage 62, 1924–1938. https://doi.org/10.1016/j.neuroimage.2012.06.005.

Sone, D., Sato, N., Ota, M., Maikusa, N., Kimura, Y., Matsuda, H., 2018. Abnormal neurite density and orientation dispersion in unilateral temporal lobe epilepsy detected by advanced diffusion imaging. Neuroimage Clin 20, 772–782. https://doi.org/10.1016/j.nicl.2018.09.017.

Steven, A.J., Zhuo, J., Melhem, E.R., 2014. Diffusion kurtosis imaging: an emerging technique for evaluating the microstructural environment of the brain. AJR Am. J. Roentgenol. 202, W26–W33. https://doi.org/10.2214/AJR.13.11365.

Tabesh, A., Jensen, J.H., Ardekani, B.A., Helpern, J.A., 2011. Estimation of tensors and tensor-derived measures in diffusional kurtosis imaging. Magn. Reson. Med. 65, 823–836. https://doi.org/10.1002/mrm.22655.

Thom, M., Eriksson, S., Martinian, L., Caboclo, L.O., McEvoy, A.W., Duncan, J.S., Sisodiya, S.M., 2009. Temporal lobe sclerosis associated with hippocampal sclerosis in temporal lobe epilepsy: neuropathological features. J. Neuropathol. Exp. Neurol. 68, 928–938. https://doi.org/10.1097/NEN.0b013e3181b05d67.

Tournier, J.D., Calamante, F., Connelly, A., 2010. Improved probabilistic streamlines tractography by 2nd order integration over fibre orientation distributions. in: Proceedings of the international Society for Magnetic Resonance in Medicine. Ismrm.

Tournier, J.-D., Mori, S., Leemans, A., 2011. Diffusion tensor imaging and beyond. Magn. Reson. Med. 65, 1532–1556. https://doi.org/10.1002/mrm.22924.

Tournier, J.-D., Calamante, F., Connelly, A., 2012. MRtrix: Diffusion tractography in crossing fiber regions. Int. J. Imaging Syst. Technol. 22, 53–66. https://doi.org/10.1002/ima.22005.

Veraart, J., Fieremans, E., Novikov, D.S., 2016. Diffusion MRI noise mapping using random matrix theory. Magn. Reson. Med. 76, 1582–1593. https://doi.org/10.1002/mrm.26059.

Winkler, A.M., Ridgway, G.R., Webster, M.A., Smith, S.M., Nichols, T.E., 2014. Permutation inference for the general linear model. Neuroimage 92, 381–397. https://doi.org/10.1016/j.neuroimage.2014.01.060.

Winston, G.P., Vos, S.B., Caldairou, B., Hong, S.-J., Czech, M., Wood, T.C., Wastling, S.J., Barker, G.J., Bernhardt, B.C., Bernasconi, N., Duncan, J.S., Bernasconi, A., 2020. Microstructural imaging in temporal lobe epilepsy: Diffusion imaging changes relate to reduced neurite density. Neuroimage Clin 26, 102231. https://doi.org/10.1016/j.nicl.2020.102231.

Wong, C., Gallate, J., 2012. The function of the anterior temporal lobe: a review of the empirical evidence. Brain Res. 1449, 94–116. https://doi.org/10.1016/j.brainres.2012.02.017.

Wu, E.X., Cheung, M.M., 2010. MR diffusion kurtosis imaging for neural tissue characterization. NMR Biomed. 23, 836–848. https://doi.org/10.1002/nbm.1506.

Wu, Y.-C., Field, A.S., Whalen, P.J., Alexander, A.L., 2011. Age- and gender-related changes in the normal human brain using hybrid diffusion imaging (HYDI). Neuroimage 54, 1840–1853. https://doi.org/10.1016/j.neuroimage.2010.09.067.

Yeatman, J.D., Dougherty, R.F., Myall, N.J., Wandell, B.A., Feldman, H.M., 2012. Tract profiles of white matter properties: automating fiber-tract quantification. PLoS One 7, e49790. https://doi.org/10.1371/journal.pone.0049790.